A Non-Orthogonal Waveform Enabled Spectrally Efficient Over-the-Air ISAC Transmission

Yu Zhang*, Tongyang Xu*, Christos Masouros†, and Izzat Darwazeh†
*School of Engineering, Newcastle University, Newcastle upon Tyne NE1 7RU, United Kingdom
†Department of Electronic and Electrical Engineering, University College London, London WC1E 6BT, United Kingdom
Email: yu.zhang@newcastle.ac.uk, tongyang.xu@newcastle.ac.uk, c.masouros@ucl.ac.uk, i.darwazeh@ucl.ac.uk

***Abstract*—This paper presents an experimental investigation into the feasibility of non-orthogonal waveform design for integrated sensing and communications (ISAC) systems. The integration of sensing and communication functionalities in wireless systems holds promise for enhancing spectral efficiency and enabling diverse applications. We propose a novel approach utilizing non-orthogonal waveforms, termed spectrally efficient frequency division multiplexing (SEFDM), to facilitate sensing and communication tasks. The system model encompasses multi-user MIMO-SEFDM communication and digital MIMO radar sensing, considering both omnidirectional and directional beamforming scenarios. We formulate an optimization problem to balance performance between communication and sensing functions. Moreover, communication performance trade-offs between orthogonal and non-orthogonal signal waveforms are studied. Through practical experiments conducted on an established over-the-air experimental platform, we evaluate the performance of the proposed ISAC waveform design and showcase the performance benefits of non-orthogonal waveform design in improving spectral efficiency, sensing beampattern accuracy, and communication quality.**

***Index Terms*—ISAC, waveform, SEFDM, MIMO, spectral efficiency, proof-of-concept, experiment.**

I. Introduction

Integrated sensing and communication (ISAC) [1] has emerged as a promising technology in 6G to enhance communication spectral efficiency and enable a wide range of sensing applications. In smart transportation, ISAC techniques enable base stations to serve as radar sensors, facilitating real-time traffic monitoring and intruder detection. For unmanned aerial vehicle (UAV) operations [2], [3], ISAC-equipped base stations offer imaging, mapping, and environmental sensing, assisting the UAV trajectory design. In medical applications, especially with Terahertz imaging, ISAC technology holds promise for disease detection and diagnosis. By merging sensing capabilities into communication systems, ISAC-based platforms offer crucial diagnostic support, enhancing patient care. Moreover , ISAC proves to be valuable in indoor environments for monitoring human movements and behaviors using wireless signals from indoor base stations or Wi-Fi networks. This facilitates the occupancy detection and activity monitoring for enhanced building management and security.

Recent studies in ISAC have explored various significant areas, such as waveform design, the exploration of information theoretical limits, and performance analysis trade-offs. Waveform designs in ISAC research can be divided into three categories: communication-based, sensing-based, and dual-functional waveform designs. Communication-based waveforms [4] involve the modification of traditional communication waveforms for radar detection purposes. Sensing-based waveform strategies [5] rely on embedding information into conventional radar waveforms, expanding the utility of radar systems. Dual-functional waveform design [6], [7] aims to optimize transmit signals to achieve a balance between sensing and communication functionalities.

From an information theory perspective, researchers have developed analytical frameworks for ISAC, simplifying the evaluation of sensing and communication performance from a mutual information (MI) perspective [8]. Optimization efforts target enhancing ISAC system performance, including extending beamforming designs to incorporate full-duplex capabilities [9], aiming to improve spectral efficiency while minimizing power consumption and maximizing sum rate. Rate-splitting of ISAC systems utilizes the Pareto optimization framework to characterize achievable performance regions considering both communication user sum rate and radar target positioning error bounds [10]. Integration of non-orthogonal multiple access (NOMA) with ISAC has emerged as a promising technique, leveraging NOMA's capacity-enhancing capabilities to enhance spectral efficiency and user connectivity [11]. ISAC-NOMA accommodates more users through superimposed NOMA communication signals, achieving high spectral efficiency and effective sensing power.

While most existing works focus on OFDM signals, the utilization of non-orthogonal multicarrier schemes, such as spectrally efficient frequency division multiplexing (SEFDM) [12], shows promise in enhancing spectral efficiency. SEFDM signal has the advantage of bandwidth savings and increased data rates compared to traditional OFDM signals. As shown in Fig. 1, SEFDM Type-I can save bandwidth by reducing subcarrier spacing while maintaining the same transmission rate per subcarrier, while SEFDM Type-II can increase the data rate while maintaining the same occupied signal bandwidth as OFDM. In this paper, we propose a multi-user MIMO-SEFDM ISAC architecture and experimentally verify the benefits of SEFDM waveforms in enhancing spectral efficiency in ISAC systems. Our contributions aim to advance the understanding of ISAC systems in signal waveform trade-offs and evaluate their practical capability in spectral efficiency improvement.

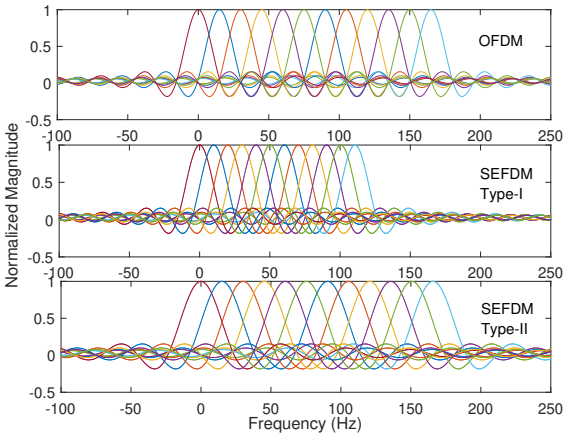

Fig. 1. Sub-carrier allocation schemes for different multicarrier signals. (1) OFDM: 12 sub-carriers, data rate R_b; (2) SEFDM Type-I: 12 sub-carriers, bandwidth compression factor α, data rate R_b; (3) SEFDM Type-II: 12 sub-carriers, bandwidth compression factor α, data rate R_b/α.

II. System Model

A. Communication Transmission Model

We consider a multi-user MIMO-SEFDM communication system. The SEFDM signal, generated with N subcarriers and Δf subcarrier spacing, is given by [13]

$$x(t) = \frac{1}{\sqrt{T}} \sum_{l=-\infty}^{\infty} \sum_{n=0}^{N-1} s_{l,n} \exp\left[\frac{j2\pi n\alpha(t-lT)}{T}\right], \quad (1)$$

where T is one SEFDM symbol duration period, $\alpha = \Delta f T$ denotes the bandwidth compression factor, and $s_{l,n}$ is a symbol modulated on the n-th subcarrier in the l-th SEFDM symbol, such as QAM or QPSK. The bandwidth compression factor α is dependent on the value of SEFDM subcarrier spacing Δf. In general, the SEFDM subcarrier spacing is smaller than that of OFDM, i.e., $0 < \alpha < 1$. The bandwidth saving percentage is $(1-\alpha) \times 100\%$. The smaller the value of α means the higher the proportion of bandwidth savings. When $\alpha = 1$, the SEFDM symbol becomes an OFDM symbol.

To derive the discrete version of SEFDM signal, we can sample $x(t)$ at T/Q intervals, as follows

$$X[k] = \frac{1}{\sqrt{Q}} \sum_{n=0}^{N-1} s_n \exp\left(\frac{j2\pi\alpha kn}{Q}\right), \quad (2)$$

where $Q = \rho N$ denotes the number of time samples and $\rho \geq 1$ is the oversampling factor. The matrix form of SEFDM signal in (2) can be expressed as

$$\mathbf{x} = \mathbf{F}\mathbf{s}, \quad (3)$$

where $\mathbf{x} \in \mathbb{C}^{Q\times 1}$ is an SEFDM symbol vector, $\mathbf{F}$ is a $Q \times N$ subcarrier matrix with elements $\exp(\frac{j2\pi\alpha kn}{Q})$, and $\mathbf{s}$ denotes an N-dimensional symbol vector. The received signal at the user is expressed as

$$\mathbf{y} = \mathbf{F}\mathbf{s} + \mathbf{w}, \quad (4)$$

where $\mathbf{w}$ is the white Gaussian noise added to the signal.

The received signal may be subject to channel effects when multiple antennas are deployed in the system. In the context of the multi-user MIMO-SEFDM transmission, the received signal can generally be expressed as [7]

$$\mathbf{Y} = \mathbf{H}\tilde{\mathbf{X}} + \mathbf{W}, \quad (5)$$

where $\mathbf{H} \in \mathbb{C}^{K\times M}$ is a MIMO channel matrix with M transmit antennas and K receive users, $\tilde{\mathbf{X}} = [\tilde{\mathbf{x}}_1, \tilde{\mathbf{x}}_2, ..., \tilde{\mathbf{x}}_M] \in \mathbb{C}^{M\times Q}$ is the precoded transmission symbol with Q time samples per data stream, and $\tilde{\mathbf{x}} \in \mathbb{C}^{Q\times 1}$ is the precoded symbol. To gain intuition on how precoding impacts the received signal, we can reformulate (5) as follows:

$$\mathbf{Y} = \mathbf{X} + \mathbf{W} + \underbrace{\left(\mathbf{H}\tilde{\mathbf{X}} - \mathbf{X}\right)}_{\text{MUI}}, \quad (6)$$

where $\mathbf{X} = [\mathbf{x}_1, \mathbf{x}_2, ..., \mathbf{x}_K]^T \in \mathbb{C}^{K\times Q}$ represents the ideal SEFDM symbol matrix that K users aim to receive. The term $\mathbf{H}\tilde{\mathbf{X}} - \mathbf{X}$ is referred to as multi-user interference (MUI), and the total power of MUI is computed as

$$P_{\text{MUI}} = \left\|\mathbf{H}\tilde{\mathbf{X}} - \mathbf{X}\right\|_F^2, \quad (7)$$

where $\|\cdot\|_F^2$ is the Frobenius matrix norm. Obviously, the value of P_{MUI} indicates the quality of precoding. We can optimize $\tilde{\mathbf{X}}$ to minimize the P_{MUI}, which will be discussed in the following sections.

B. MIMO Radar Sensing Model

In this paper, we consider a digital MIMO radar system which has a higher degree of freedom compared to the traditional analog phased-array radar. The sensing beampattern of digital MIMO radar is determined by the spatial covariance matrix of $\tilde{\mathbf{X}}$ [14]. Without loss of generality, we present the design of both omnidirectional and directional MIMO radar waveforms while also considering the implications for communication transmission.

1) Omnidirectional beampattern: To generate an omnidirectional beampattern, the transmission waveform matrix $\tilde{\mathbf{X}}$ must be orthogonal, resulting in the covariance matrix of $\tilde{\mathbf{X}}$ being an identity matrix. The optimization problem is formulated as follows

$$\min_{\tilde{\mathbf{X}}} \quad \left\|\mathbf{H}\tilde{\mathbf{X}} - \mathbf{X}\right\|_F^2 \quad (8)$$

$$\text{s.t.} \quad \frac{1}{Q}\tilde{\mathbf{X}}\tilde{\mathbf{X}}^H = \frac{P_T}{M}\mathbf{I}_M, \quad (8a)$$

where P_T is the total transmit power and $\mathbf{I}_M$ is an $M \times M$ identity matrix.

2) Directional beampattern: For a directional beampattern, the covariance matrix $\mathbf{R}_d$ is positive-definite and $Q \geq M$. The optimization problem for the directional MIMO radar is expressed as

$$\min_{\tilde{\mathbf{X}}} \quad \left\|\mathbf{H}\tilde{\mathbf{X}} - \mathbf{X}\right\|_F^2 \quad (9)$$

$$\text{s.t.} \quad \frac{1}{Q}\tilde{\mathbf{X}}\tilde{\mathbf{X}}^H = \mathbf{R}_d. \quad (9a)$$

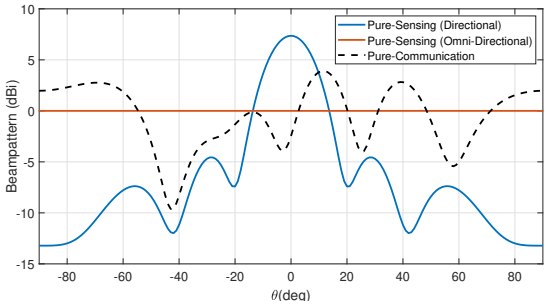

Fig. 2. Sensing beampattern illustration for pure-communication systems (γ=1) and pure-sensing systems (γ=0) considering directional and omnidirectional beampatterns.

C. Trade-off Between Communication and Sensing

To balance performance between communication and sensing, we introduce a trade-off factor γ and the desired sensing signal X_d. Thus, the dual-functional sensing and communication optimization problem can be expressed as follows:

$$\min_{\tilde{\mathbf{X}}} \quad \gamma \left\| \mathbf{H}\tilde{\mathbf{X}} - \mathbf{X} \right\|_F^2 + (1-\gamma) \left\| \tilde{\mathbf{X}} - \mathbf{X}_d \right\|_F^2 \tag{10}$$

$$\text{s.t.} \quad \frac{1}{Q} \left\| \tilde{\mathbf{X}} \right\|_F^2 = P_T. \tag{10a}$$

When the trade-off factor γ equals 0, (10) tends to represent a pure sensing optimization problem. Conversely, when γ equals 1, the sensing component in (10) is eliminated, transforming it into a pure communication system. The beampatterns for $\gamma = 1$ and $\gamma = 0$ are presented in Fig. 2. By adjusting the trade-off factor, we can achieve the desired balance between communication and sensing performance according to specific application scenarios.

III. Experiment Design for Multiuser-MIMO SEFDM-ISAC System

In our experiment, we designed and implemented a platform to evaluate how variations in the error vector magnitude (EVM) and the quality of sensing beampattern are influenced by adjustments in two factors: the trade-off factor γ and the bandwidth compression factor α. As depicted in Fig. 3(a), the Tx-USRP array serves as a base station, which consists of six transmit antennas arranged in a uniform linear array (ULA) format at the top of the testbed, with a spacing of half a wavelength. There are two RF chains in each USRP: one for signal generation and the other for signal reception. In this experiment, we utilize one RF chain from each USRP to generate a signal at a carrier frequency of 2.4 GHz. Both OFDM and SEFDM signals employ 128 subcarriers and each sub-carrier is modulated with quadrature phase shift keying (QPSK) symbols. The experimental scenario includes two communication users (CUs), each equipped with an omnidirectional antenna and connected to a USRP for signal reception, as shown in Fig. 3(b). The layout of the experiment setup is in Fig. 3(c). The base station and the users are placed around 1.7m apart, with a 20cm distance separating the two users.

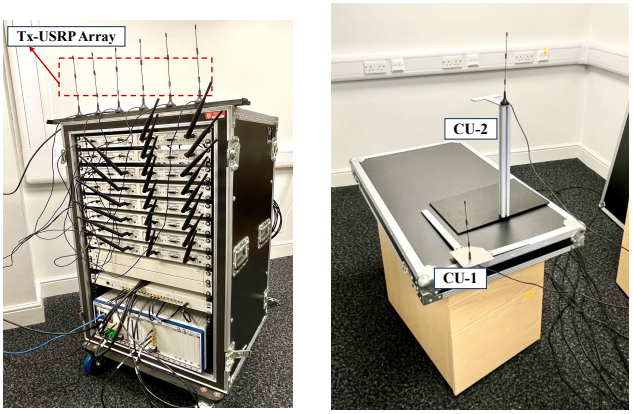

(a) Tx-USRP array with 6 transmit antennas (b) Two single-antenna users

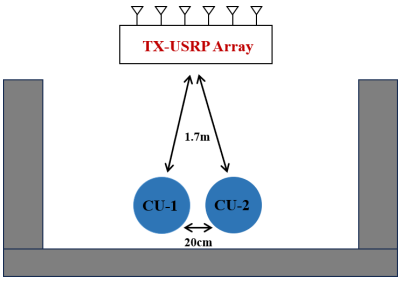

(c) Loboratory floor plan

Fig. 3. The multiuser-MIMO SEFDM-ISAC experiment platform setup.

Given the indoor nature of our experiment, some objects can cause signal reflection and blocking, resulting in multipath propagation. To address the multipath effects, we employ frequency-domain channel estimation and equation techniques. Furthermore, to tackle the challenges posed by non-orthogonal signal interference and the MIMO antenna interference, we employ waveform precoding and MIMO space precoding algorithms [15]. To assess the trade-off performance between communication and sensing, we set the value of γ to 1, 0.9, and 0.5. For evaluating the trade-off performance between orthogonal OFDM and non-orthogonal SEFDM signals, we consider α values of 1, 0.9, 0.8, and 0.7.

IV. Measurement Results

In this section, we present the experimental results considering the trade-off between communication and sensing, as well as the performance of non-orthogonal waveforms.

The measured results for the omnidirectional beam are shown in Fig. 4. It is evident that as γ decreases, the omnidirectional beampattern improves. Particularly at $\gamma = 0.5$, we achieve an almost perfect omnidirectional radar beampattern. The communication performance is not only affected by the trade-off factor γ but also by the non-orthogonal waveform bandwidth compression factor α. In Fig. 4(a), where the trade-off factor $\gamma = 1$, it represents a pure communication system. The QPSK constellation becomes scattered and the EVM performance deteriorates as α decreases, indicating that SEFDM improves bandwidth efficiency at the expense of

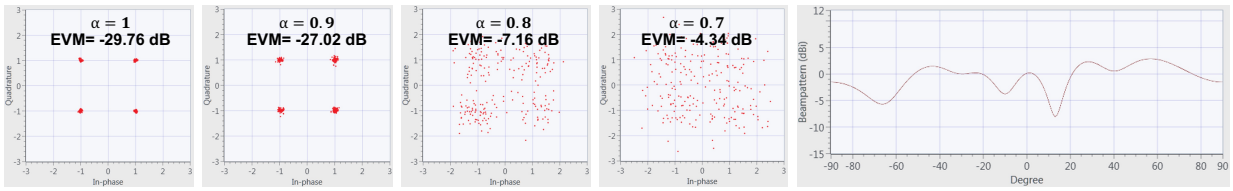

(a) $\gamma = 1$, omnidirectional beam

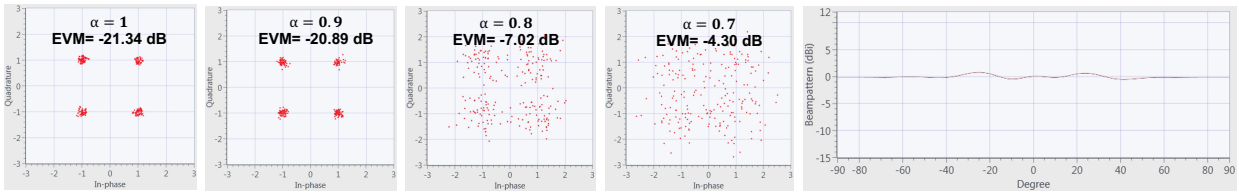

(b) $\gamma = 0.9$, omnidirectional beam

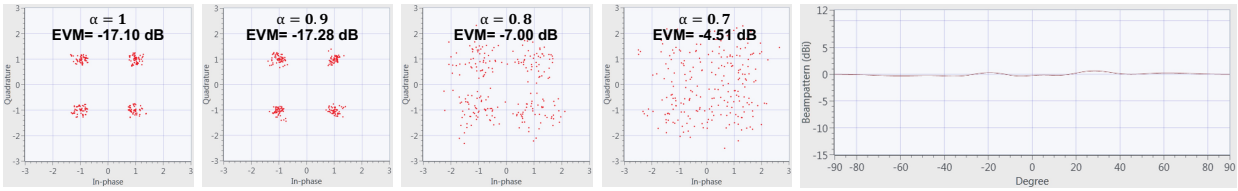

(c) $\gamma = 0.5$, omnidirectional beam

Fig. 4. EVM performance and omnidirectional beampattern under different bandwidth compression factors α and trade-off factors γ.

communication performance. By comparing Fig. 4(a), Fig. 4(b), and Fig. 4(c), we observe that in the case of $\alpha = 1$ (OFDM signal), the EVM performance deteriorates rapidly as γ decreases. However, in the cases of $\alpha = 0.8$ or $\alpha = 0.7$, we observe that the EVM performance does not exhibit significant changes as γ decreases. This result suggests that the SEFDM signal exhibits better robustness to changes in omnidirectional radar sensing performance.

In Fig. 5, we present the measurement results for the directional beam. Unlike the flat beampattern in the omnidirectional system, a desirable beampattern for the directional system is a clear beam with a high peak-to-sidelobe ratio (PSLR). It can be observed that when $\gamma = 0.9$, we can already obtain a clear directional beampattern with a PSLR of 7 dB. This means that for the directional beam system, we can guarantee sensing performance with little sacrifice of communication performance. Through comparison with Fig. 5(a), Fig. 5(b), and Fig. 5(c), we can conclude that when $\alpha = 0.8, 0.7$, the EVM performance has little changes with different γ. Nevertheless, when $\alpha = 1, 0.9$, the EVM performance is severely affected by changes in γ. Similar to the omnidirectional system, the SEFDM signal in the directional system also exhibits better robustness to changes in the trade-off factor.

Fig. 6 illustrates the EVM performance of omnidirectional and directional beams under varying γ. As anticipated, the EVM performance improves for both omnidirectional and directional beams as γ increases. It is notable from the figure that the EVM performance of the omnidirectional beam surpasses that of the directional beam. This difference in performance could be attributed to the inherent characteristics of omnidirectional and directional beams. Omnidirectional beams transmit signals uniformly in all directions, resulting in less signal degradation or interference. Directional beams focus signals in a specific direction and may experience more signal degradation or interference, especially at off-axis angles, which can lead to poorer EVM performance.

V. Conclusion

We propose a multiuser-MIMO SEFDM-ISAC framework and address the experimental proof of non-orthogonal waveform design for ISAC systems Based on the conducted experiments and analysis, we can adjust the trade-off factor and bandwidth compression factor to meet the requirement for the performance of communication and sensing in specific application scenarios. The experimental validation provides valuable insights for optimizing ISAC systems to achieve enhanced spectral efficiency, communication quality, and sensing accuracy. By bridging the gap between theoretical analysis and practical experimentation, this work paves the way for further exploration and innovation in ISAC technologies.

VI. Acknowledgement

This work was supported in part by the UK Engineering and Physical Sciences Research Council (EPSRC) under Grant EP/Y000315/1, and in part by HORIZON-SNS-2023: 6G-Multiband Wireless and Optical Signalling for Integrated Communications, Sensing and Localisation (6G-MUSICAL).

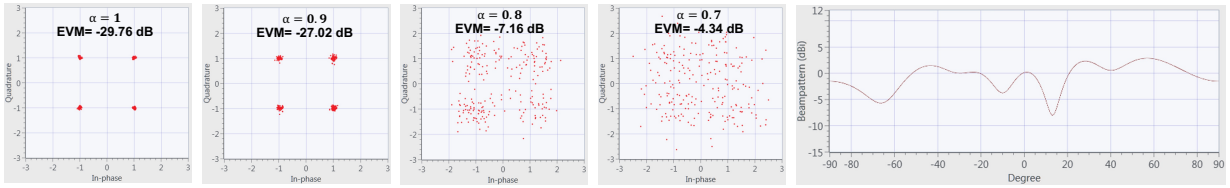

(a) $\gamma = 1$, directional beam

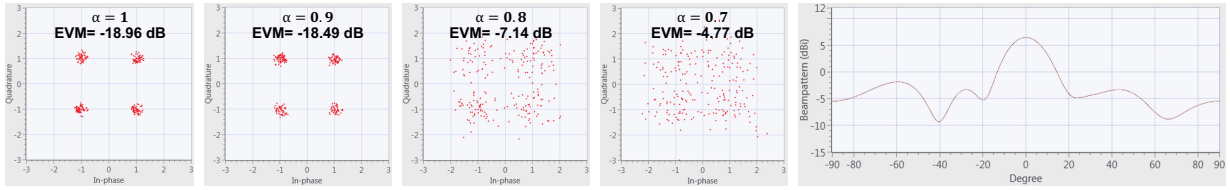

(b) $\gamma = 0.9$, directional beam

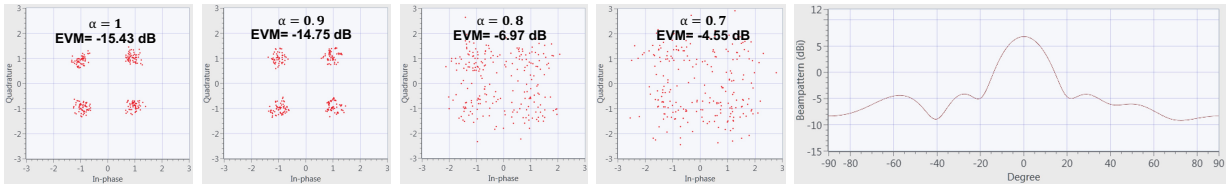

(c) $\gamma = 0.5$, directional beam

Fig. 5. EVM performance and directional beampattern under different bandwidth compression factors α and trade-off factors γ.

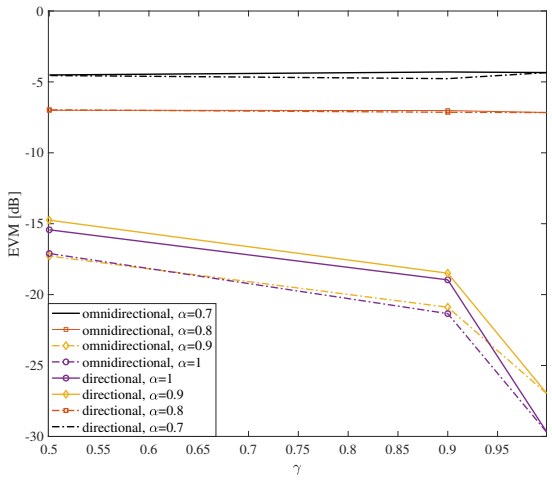

Fig. 6. EVM performance for omnidirectional and directional beam patterns with different γ.

REFERENCES

[1] International Telecommunication Union, "IMT towards 2030 and beyond," Jun. 2023. [Online]. Available: https://www.itu.int/en/ITU-R/study-groups/rsg5/rwp5d/imt-2030/Pages/default.aspx

[2] Z. Jia, Q. Wu, C.Dong, C. Yuen, and Z. Han, "Hierarchical aerial computing for Internet of things via cooperation of HAPs and UAVs," *IEEE Internet Things J.,* vol. 10, no. 7, pp. 5676–5688, Apr. 2023.

[3] Y. Zhang, Z. Mou, F. Gao, J. Jiang, R. Ding, and Z. Han, "UAV-enabled secure communications by multi-agent deep reinforcement learning," *IEEE Trans. Veh. Technol.,* vol. 69, no. 10, pp. 11599–11611, Oct. 2020.

[4] C. Sturm, T. Zwick, and W. Wiesbeck, "An OFDM system concept for joint radar and communications operations," in *Proc. IEEE 69th Veh. Technol. Conf. (VTC Spring)*, Barcelona, Spain, Jun. 2009, pp. 1–5.

[5] J. Xiong, H. Yin, J. Zhu, and Y. Tang, "An overview of waveform design for integrated sensing and communication," in *Proc. IEEE/CIC Int. Conf. Commun. China (ICCC),* 2022, pp. 991–996.

[6] F. Liu, L. Zhou, C. Masouros, A. Li, W. Luo, and A. Petropulu, "Toward dual-functional radar-communication systems: Optimal waveform design," *IEEE Trans. Signal Process.,* vol. 66, no. 16, pp. 4264–4279, Aug. 2018.

[7] T. Xu, F. Liu, C. Masouros, and I. Darwazeh, "An experimental proof of concept for integrated sensing and communications waveform design," *IEEE open J. Commun. Soc.,* vol. 3, pp. 1643–1655, Sep. 2022.

[8] C. Ouyang, Y. Liu, H. Yang, and N. Al-Dhahir, "Integrated sensing and communications: A mutual information-based framework," *IEEE Commun. Mag.,* vol. 61, no. 5, pp. 26–32, May 2023.

[9] Z. He, W. Xu, H. Shen, D. W. K. Ng, Y. C. Eldar, and X. You, "Full-duplex communication for ISAC: Joint beamforming and power optimization," *IEEE J. Sel. Areas Commun.,* vol. 41, no. 9, pp. 2920–2936, Sep. 2023.

[10] P. Gao, L. Lian, and J. Yu, "Cooperative ISAC with direct localization and rate-splitting multiple access communication: A Pareto optimization framework," *IEEE J. Sel. Areas Commun.,* vol. 41, no. 5, May 2023.

[11] Z. J. Wang, Y. Liu, X. Mu, Z. Ding, and O. A. Dobre, "NOMA empowered integrated sensing and communication," *IEEE Commun. Lett.,* vol. 26, no. 3, pp. 677–681, Mar. 2022.

[12] I. Darwazeh, T. Xu, T. Gui, Y. Bao, and Z. Li, "Optical SEFDM system; bandwidth saving using non-orthogonal sub-carriers," *IEEE Photon. Technol. Lett.,* vol. 26, no. 4, pp. 352–355, Feb. 2014.

[13] T. Xu and I. Darwazeh, "Transmission experiment of bandwidth compressed carrier aggregation in a realistic fading channel," *IEEE Trans. Veh. Technol.,* vol. 66, no. 5, pp. 4087–4097, May 2016.

[14] D. R. Fuhrmann and G. S. Antonio, "Transmit beamforming for MIMO radar systems using signal cross-correlation," *IEEE Trans. Aerosp. Electron. Syst.,* vol. 44, no. 1, pp. 171–186, Jan. 2008.

[15] T. Xu and C. Masouros and I. Darwazeh, "Waveform and Space Precoding for Next Generation Downlink Narrowband IoT," *IEEE open J. Commun. Soc.,* vol. 6, pp. 5097–5107, 2019.